This ESI for *J. Mater. Chem. A,* 2019, **7**, 2027-2033, originally published on 7th January 2019, was updated on 22nd April 2020 to address formatting issues with Fig. S4, S6, S8 and S10.

Supporting Information

3D Morphological Stability of P3HT Nanowire-Based Bulk Heterojunction Thin Films against Light Irradiation Quantitatively Resolved by TEM Tomography

Seon-Mi Jin,[a,b] Jinwoo Nam,[a,b] Chang Eun Song,[c] Heesun Chung,[b] BongSoo Kim,[d] Eunji Lee[*,a]

[a] School of Materials Science and Engineering, Gwangju Institute of Science and Technology (GIST), Gwangju 61005, Republic of Korea

[b] Graduate School of Analytical Science and Technology, Chungnam National University, Daejeon 34134, Republic of Korea

[c] Center for Solar Energy Materials, Korea Research Institute of Chemical Technology (KRICT), Daejeon 34114, Republic of Korea

[d] Department of Chemistry, Ulsan National Institute of Science and Technology (UNIST), Ulsan 44919, Republic of Korea

Corresponding Author

E-mail: eunjilee@gist.ac.kr

1. Materials and Instruments All commercially available reagents were used without further purification unless otherwise indicated. 1,2-Bis(diphenylphosphinoethane)nickel(II) chloride [Ni(dppp)Cl_2] was purchased from Sigma-Aldrich Chemical Co., Ltd., and palladium(II) acetate [$Pd(OAc)_2$] was purchased from Kawaken Fine Chemicals Co. Ltd. Bis(triphenylphosphine)nickel(II) chloride [$(PPh_3)_2NiCl_2$] was purchased from TCI Chemical Co. Ltd., and stored in a vacuum atmosphere glovebox under nitrogen. The [6,6]-phenyl-C_{71}-butyric acid methyl ester ($PC_{71}BM$) was purchased from Nano-C, and the poly(3,4-ethylenedioxythiophene):poly(styrenesulfonate) (PEDOT:PSS) was purchased from Heraeus Co. Zinc acetate dehydrate, ethanolamine, 2-methoxyethanol, ethoxylated polyethylenimine (PEIE), and MoO_3 were supplied by Sigma-Aldrich Chemical Co. Ltd..

Nuclear Magnetic Resonance (NMR) Spectrometer. ^{1}H NMR spectra were recorded at 500 MHz using $CDCl_3$ as a solvent. The chemical shifts of all ^{1}H NMR spectra were referenced to the residual signal of $CDCl_3$ (δ 7.26 ppm) using Bruker 250 MHz and 500 MHz NMR instruments. All coupling constants, *J*, are reported in Hertz (Hz).

Gel Permeation Chromatography (GPC). The GPC measurements were performed on a Waters RI system equipped with a UV detector, a differential refractometer detector, and an Ultra styragel linear column at 35 °C using THF (HPLC grade) as the eluent. The molecular weight (M_n) and the polydispersity index (PDI) values were calculated using monodisperse polystyrene standards.

UV-Vis and Fluorescence Spectrometer. Absorption spectra were obtained using a UV-Vis spectrometer (NEOSYS-2000, Scinco, Seoul, Republic of Korea). The emission spectra were characterized by fluorescence spectrometer (FS-2, Scinco, Seoul, Republic of Korea).

Raman Spectrometer. Raman spectra were obtained using a laser operating at a wavelength of 532 nm with a spectral resolution of 1.4 cm^{-1} (FEX, NOST, Seongnam, Republic of Korea).

Fourier Transform Infrared (FT-IR) Spectrometer. FT-IR spectra were recorded on VERTEX 80v (Bruker Optic GmbH, Bremen, Germany) using a ZnSe window.

Transmission Electron Microscopy (TEM). For TEM samples, the polymer blend solutions with $PC_{71}BM$ were spin-coated on glass substrate, covered with water-soluble PEDOT:PSS. PEDOT:PSS was spun at 5000 rpm for 20 sec from a solution. All thin films on PEDOT:PSS are floated off in deionized (DI) water and transferred on a carbon-coated copper grid. The images were obtained on a JEM-1400 (JEOL, Japan) operating at 120 kV, and the images were acquired with Veleta (with a megapixel) and Tengra (with 5.3 megapixel) CCD cameras (EMSIS, Germany).

Current density-Voltage (*J-V*) Measurement System. The *J–V* characteristics were recorded using a computer-controlled Keithley 236 Source-Measure unit (Keithley Instruments, Inc., USA). The PSC performances were measured under illumination of AM 1.5 G, 100 mW/cm^2, using a solar simulator (Newport-Oriel Instruments, USA) with xenon light source.

2. Methods

P3HT NWs/$PC_{71}BM$ 1 vs. P3HT NWs/$PC_{71}BM$ 2. Two different processes using the *m*-xylene solvent, including premixing (P3HT NWs/$PC_{71}BM$ **1**) and postmixing (P3HT NWs/$PC_{71}BM$ **2**) methods, were used for the blend of P3HT and $PC_{71}BM$. The crystallization-driven assembly of P3HT into NW was induced by heating and cooling of *m*-xylene solution. The *m*-xylene was selected as a marginal solvent for P3HT.

• **Premixed P3HT NWs/$PC_{71}BM$ 1 Solution**: 10 mg of P3HT and 10 mg of $PC_{71}BM$ were dissolved in 1 mL *m*-xylene at 60 °C under agitation. During the dissolution process, the solution was protected from light and ambient air to avoid the chemical oxidation and/or the photo-oxidation of the polymer and $PC_{71}BM$. After the complete dissolution of the materials, the *m*-xylene solution was slowly cooled to room temperature.

• **Postmixed P3HT NWs/$PC_{71}BM$ 2 Solution**: 10 mg of P3HT was dissolved in 1 mL *m*-xylene at 60 °C under agitation. During the dissolution process, the solution was protected from light and ambient air to avoid the chemical oxidation and/or the photo-oxidation of the polymer. After the complete dissolution of the P3HT polymer, the solution was slowly cooled to room temperature. And then, 10 mg of $PC_{71}BM$ was added into P3HT NWs solution in *m*-xylene.

Quantitative Analysis of Aggregated P3HT Chains. The absorption spectra of each solution were normalized to the maximum absorption.[S1,2] The measured absorption spectra are composed of a high-energy region attributed to unaggregated chains and a low-energy region originated from the vibronic structure of aggregated chains.

The absorption spectrum was decomposed into a scaled unaggregated chains in chlorobenzene solution (gray dot line), and aggregate spectrum (black/red/blue dash dot line). The spectrum of unaggregated chains in chlorobenzene solution (gray dot line) was subtracted from the original spectrum (respective open symbol, solid line) containing both aggregated and unaggregated chains, resulting in the spectrum representing the dash dot line, as shown in Fig. S3. The equation is below.

$$fx(\mathrm{x}) = \frac{1}{\sqrt{2\pi}\sigma} e^{\frac{-(x-\mu)^2}{2\sigma^2}} \quad \int_{-\infty}^{\infty} fx(x)dx = 1 \quad \text{---- (1)}$$

In order to analyze the aggregation of P3HT, the relative intensity between the vibronic transitions in the absorption spectra of the P3HT solution was compared within the weak interchain coupling framework model developed by Clark et al.[S3] The ratio of the $A_{0\text{-}0}$ and $A_{0\text{-}1}$ absorbance is related to the free exciton bandwidth (*W*) of the aggregates and the energy of the main intramolecular vibration energy (*E*p) coupled to the electronic transition by the following expression (assuming a Huang-Rhys factor of 1):

$$\frac{A_{0-0}}{A_{0-1}} = \left(\frac{1-0.24W/E_p}{1+0.073W/E_p}\right)^2 \quad \text{---------- (2)}$$

Using the $A_{0\text{-}0}/A_{0\text{-}1}$ ratio from equation, and assuming the C=C symmetric stretch at 0.179 eV dominates the coupling to the electronic transition, *W* can be estimated. If the intensity ratio of the $A_{0\text{-}0}/A_{0\text{-}1}$ is smaller than 1, it is the H-type aggregated model. In contrast, if the intensity ratio of the $A_{0\text{-}0}/A_{0\text{-}1}$ is larger than 1, it is the J-type aggregated model.

Fabrication of P3HT NWs/$PC_{71}BM$ 1 and 2 Thin Films. The glass substrates were sequentially cleaned with DI water, acetone, and isopropanol, and dried in oven at 120 °C overnight. Then, the substrates were treated with UV/ozone for 15 min. A thin film of PEDOT:PSS was spin-coated at 5000 rpm for 20 sec and annealed at 150 °C for 15 min. The NW blend solutions (P3HT:$PC_{71}BM$=1:1 (w/w), 20 mg/mL in *m*-xylene) was spin-coated at 1200 rpm for 15 sec on the PEDOT:PSS glass. The thickness of the photoactive films was fixed about ~100 nm.

Light Irradiation System.[S4] The films were exposed to continuous illumination by a halogen lamp of Philips MR16 50W for 1 day under air. All samples were placed on a bottom platform that ensured each sample had the same average irradiation intensity.

3D Construction of NWs-Based Films by Transmission Electron Microscopy Tomography (TEMT). Experimental data for TEMT were obtained by JEM-1400 (JEOL, Japan) operating at 120 kV. The current density of electron beam remained constantly at 19.7 pA/cm^2. The tilt series of TEM images were recorded with a 1 sec exposure time using a Veleta or a Tengra CCD camera. Tilting, refocusing, and repositioning were carried out after every individual tilt increase. Alignment and reconstruction of tilt series were performed in IMOD software. 3D visualization and quantitative analysis of the final volumes were carried out using Amira 6.0 visualization software from FEI. Nonlinear anisotropic diffusion filter was used to reduce the noise, segmentation of the reconstruction of the NWs-based films. The specific slicing plane in the reconstructed volume with 101.16 nm thickness was selected to explain the 3D morphology of P3HT/$PC_{71}BM$ and P3HT NWs/$PC_{71}BM$ films as shown in Fig. S7 and S9.

Table S1 Detailed experimental conditions for tomography.

Blend films	P3HT/ $PC_{71}BM$	P3HT/ $PC_{71}BM$ (after exposure to light)	P3HT NWs/ $PC_{71}BM$ **1**	P3HT NWs/ $PC_{71}BM$ **1** (after exposure to light)	P3HT NWs/ $PC_{71}BM$ **2**	P3HT NWs/ $PC_{71}BM$ **2** (after exposure to light)
Angular sampling	- 60° ~ + 60°	- 60° ~ + 60°	- 68° ~ + 62°	- 70° ~ + 70°	- 62° ~ + 60°	- 56° ~ + 68°
Increments angle	2°					
Magnification	25,000 ×					
Pixel size	2.81 nm for images					

Grazing-Incidence Wide-Angle X-ray Scattering (GI-WAXS). GI-WAXS measurement was performed on PLS-II 9A U-SAXS beamline in the Pohang Accelerator Laboratory (Republic of Korea). The X-rays generated from the in-vacuum undulator were monochromated by Si(111) double crystals and were focused on the detector position using K-B type mirror system. X-rays with a wavelength of 1.109 Å were used. The incidence angle was set to 0.12° or 0.13°. The GI-WAXS patterns were collected by a 2D CCD detector (Rayonix SX165) and then analyzed using the software of IGOR Pro. Diffraction angles were calibrated by pre-calibrated sucrose (Monoclinic, P21, a = 10.8631 Å, b = 8.7044 Å, c = 7.7624 Å, β = 102.938°) and the sample-to-detector distance was roughly 228 mm. The thin films (thickness of ~ 100 nm) were spin-cast from a solution of P3HT/$PC_{71}BM$, P3HT NWs/$PC_{71}BM$ **1**, and P3HT NWs/$PC_{71}BM$ **2** on silicon substrates. Before casting of each solution, the Si-wafer was cleaned by sonication in chloroform, acetone and isopropanol, respectively, for 20 min each. The cleaned substrate was transferred in piranha solution and heated for 1 h at 100 °C.

The crystal size and relative crystallinity were estimated by the FWHM of the (100) diffraction peak using the Debye-Scherrer equation.[S5,6]

$$t_{hkl} = \frac{0.9\,\lambda}{\beta \cos\theta_{hkl}} \quad \text{---------- (3)}$$

Where λ is the incident X-ray wavelength, t_{hkl} is the coherent crystal size, K is a dimensionless Scherrer constant (generally given as K = 0.9), β is the FWHM in radians, θ_{hkl} is the glancing angle. The evaluated crystallinity along the out-of-plane (100) are given in Table S11.

Device Fabrication and Characterization. In this study, inverted BHJ PSCs were fabricated with an ITO/ZnO/PEIE/P3HT:$PC_{71}BM$ or P3HT NWs:$PC_{71}BM$ (**1** or **2)**/MoO_3/Ag structure. The ITO glass substrates were cleaned with detergent solution and subsequently ultrasonicated in deionized water, acetone and isopropanol. The precleaned ITO substrates were treated with

UV/ozone for 20 min. The ZnO nanoparticles dispersed in isopropanol was spin-coated onto ITO glass substrates at 5000 rpm for 20 sec and dried at 100 °C for 10 min. PEIE solution was spin-coated at a speed of 5000 rpm for 20 sec and dried at 120 °C for 10 min. The P3HT:$PC_{71}BM$ and P3HT NWs:$PC_{71}BM$ blend solutions (P3HT:$PC_{71}BM$=1:1 w/w, 20 mg/ml in chlorobenzene and *m*-xylene, respectively) were spin-coated in a glove box at 1000 rpm for 30 sec on the PEIE/ZnO-coated ITO glass. The thickness of the films was fixed at ~100 nm. The device fabrication was completed by thermal evaporation of 10 nm MoO_3 and 100 nm Ag as the anode at a base pressure of 3×10^{-6} Torr. The PSC characteristics were determined by illuminating the cells with simulated AM 1.5G at 100 mW/cm^2 at room temperature. The simulator irradiance was characterized using a calibrated spectrometer, and the illumination intensity was set using an NREL-certified silicon diode with an integrated KG1 optical filter. The photo-stability of the glass-encapsulated PSCs was tested as a function of the exposure time. The devices were exposed to 100 mW/cm^2 with AM 1.5G in air (60% humidity, room temperature).

3. Synthesis

Synthesis of P3HT. Lithium diisopropylamide (LDA) was generated by addition of *n*-BuLi (2.5 M in hexane, 2.31 mL, 5.77 mmol) to a solution of diisopropylamine (1.02 mL, 7.28 mmol) in dry THF (14.6 mL, 0.5 M conc.) at -78 °C. The solution was stirred at this temperature for 1 hr. The freshly generated LDA solution was added dropwise to the 2-bromo-3-hexylthiophene (1.50 g, 6.068 mmol) in dry THF (45 mL) at -78 °C. Then $ZnCl_2$ (868 mg, 6.37 mmol) was added and the mixture was stirred at -78 °C for 30 minutes and then warmed to room temperature for 1 hr prior to the addition of Ni(dppp)Cl_2 (65.79 mg, 0.121 mmol). The reaction was then stirred overnight at room temperature. The thick purple mixture was precipitated with methanol, and the resulting precipitate was then filtered. Oligomers and impurities in the product were removed by Soxhlet extractions with methanol and hexane, followed by chloroform extraction. The polymer was recovered from the chloroform fraction, followed by concentration and finally precipitation into methanol. ^{1}H NMR (500 MHz, $CDCl_3$) δ 6.98 (s, 1H), 2.69-2.86 (m, 2H), 1.55-1.65 (m, 2H), 1.35-1.48 (m, 2H), 1.22-1.40 (m, 4H), 0.90 (t, *J* = 6.2 Hz, 3H).

Table S2 Characteristics of synthesized P3HT used in this study.

Polymer	M_n (g·mol^{-1})[a]	PDI[a]	RR(%)[b,c]
P3HT	12,700	1.21	92

[a]Determined from GPC in THF calibrated by polystyrene standards. [b]Determined from ^{1}H NMR. [c]Regioregularity of P3HT block denoted as RR.

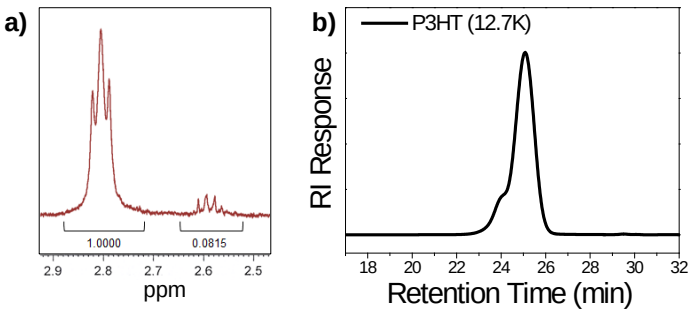

Fig. S1 a) Expanded region from ^{1}H NMR of P3HT showing the degree of regioregularity of 92%. b) GPC traces of P3HT with THF as eluent.

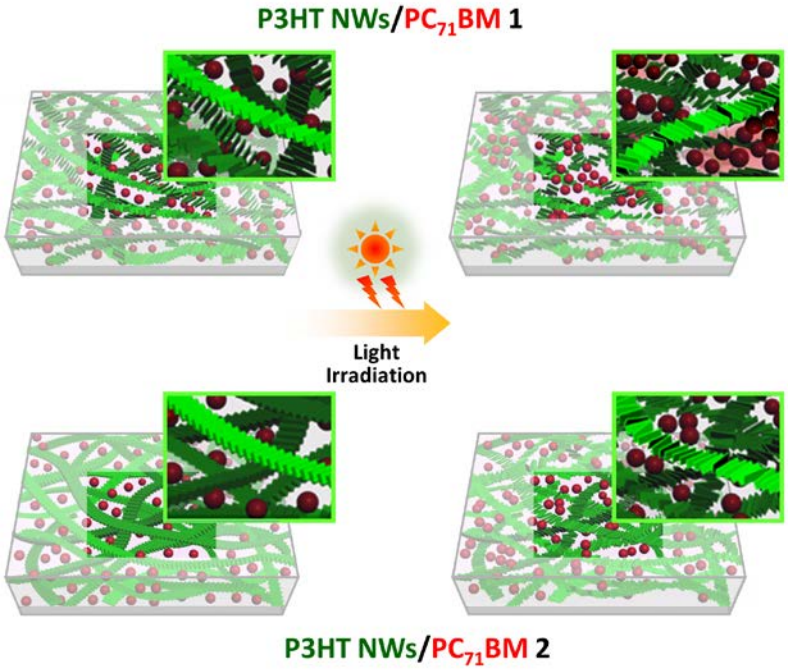

Scheme S1 Schematic representation of two different NWs-based photoactive films, P3HT NWs/$PC_{71}BM$ **1** and **2**, before and after exposure to light for 24 hr.

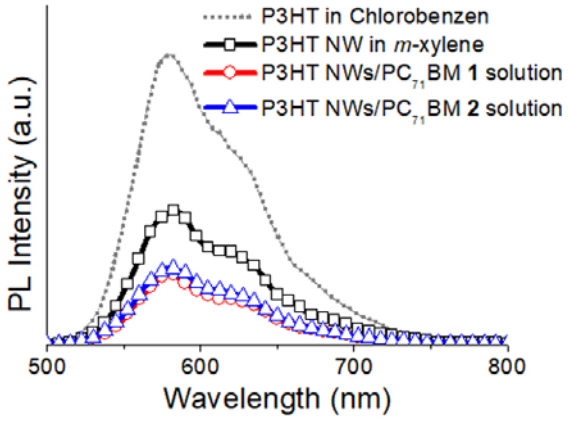

Fig. S2 Fluorescence spectra of P3HT chlorobenzene, P3HT NWs *m*-xylene, and P3HT NWs/$PC_{71}BM$ *m*-xylene solutions (0.05 mg/mL). For the fabrication of P3HT NW, the 'whisker method' was used in *m*-xylene.[S7]

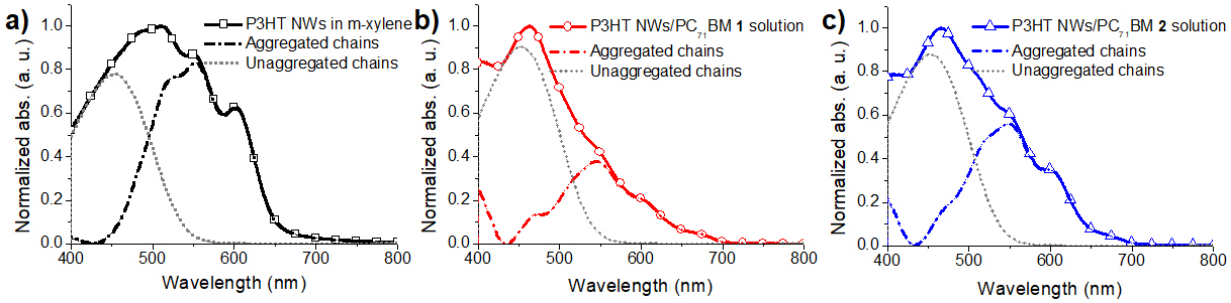

Fig. S3 Experimental absorption spectra of P3HT chlorobenzene, P3HT NWs *m*-xylene, and P3HT NWs/ $PC_{71}BM$ **1** and **2** *m*-xylene solutions. Each absorption spectrum was decomposed into scaled unaggregate chains (gray dot line), and aggregate chains (black/red/blue dash dot line) modeled as a progression of Gaussian functions.

Table S3 Fraction of unaggregated and aggregated P3HT chains for the formation of P3HT NWs (0.05 mg/mL of *m*-xylene), as calculated by absorption spectra in Fig. S3.

Methods	Unaggregated chains [%]	Aggregated chains [%]	$A_{0\text{-}0}/A_{0\text{-}1}$[a]	W[b] [Free-exciton bandwidth, eV]
Pre-assemble P3HT NWs in *m*-xylene	43.50	56.50	0.76	0.076
P3HT NWs/$PC_{71}BM$ **1** solution	64.53	35.47	0.53	0.163
P3HT NWs/$PC_{71}BM$ **2** solution	55.48	44.52	0.62	0.128

[a]Determined from the relative absorption intensity. [b]Determined by using Spano's model for weakly interacting H-aggregates.[S8]

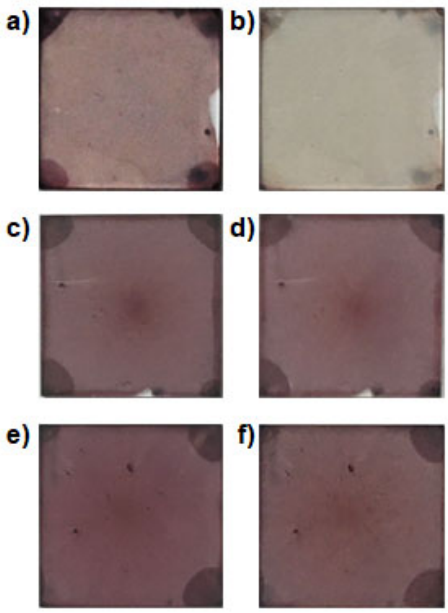

Fig. S4 Optical micrographs of as-cast thin films a,c,e) before and b,d,f) after light irradiation for 24 hr; a,b) P3HT/$PC_{71}BM$ blend films, c,d) P3HT NWs/$PC_{71}BM$ **1** films, and e,f) P3HT NWs/$PC_{71}BM$ **2** films.

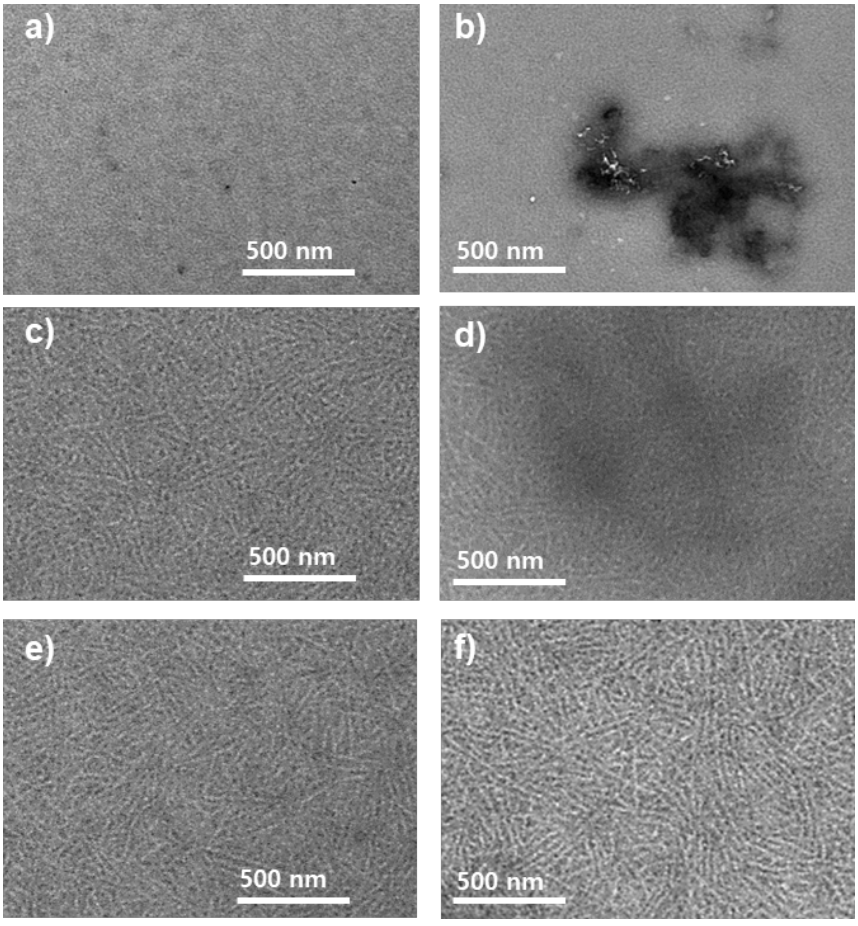

Fig. S5 TEM images of as-cast thin films a,c,e) before and b,d,f) after light irradiation for 24 hr; a,b) P3HT/$PC_{71}BM$ blend films, c,d) P3HT NWs/$PC_{71}BM$ **1** films, and e,f) P3HT NWs/$PC_{71}BM$ **2** films.

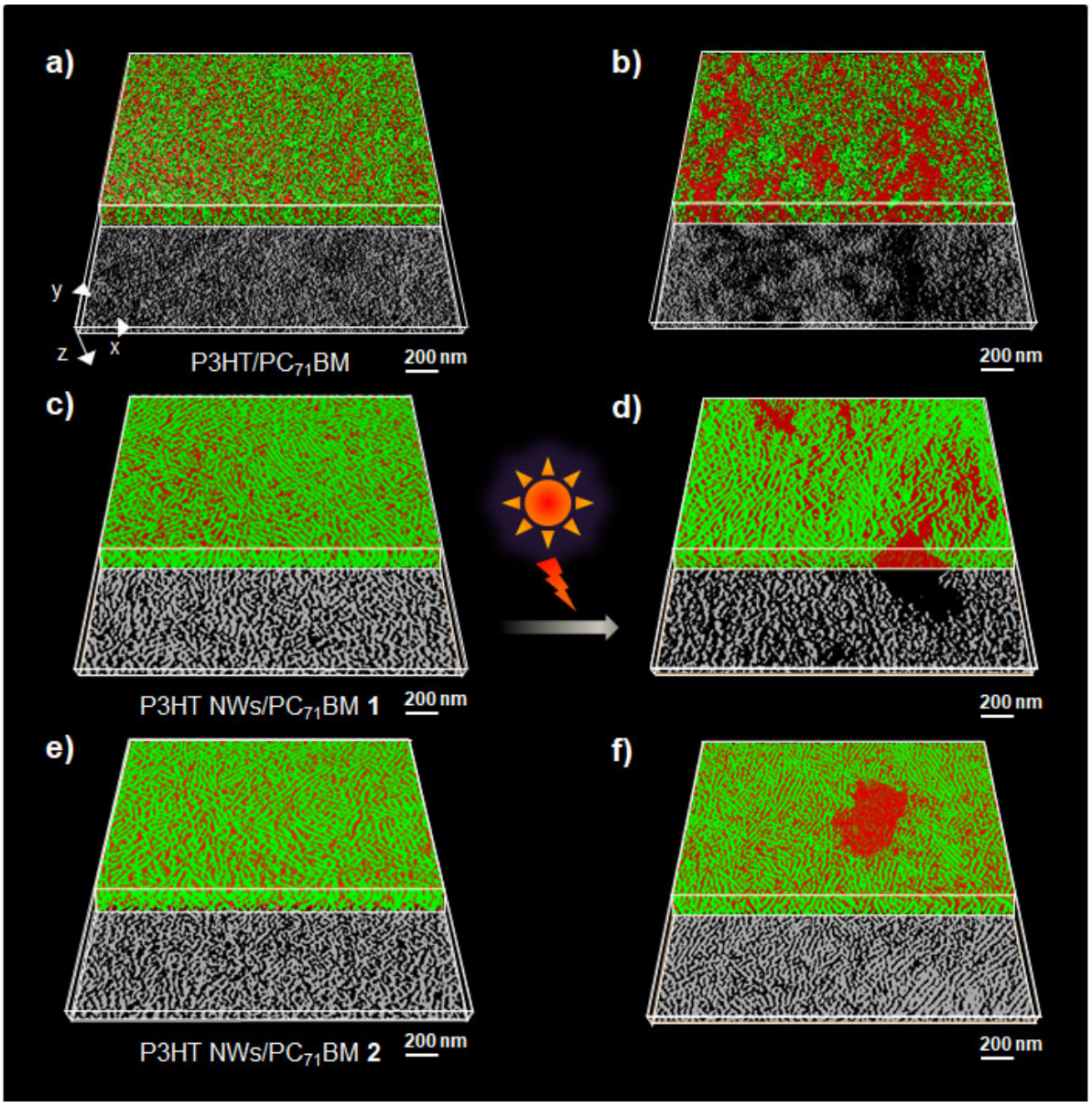

Fig. S6 The photoactive films cast from three different P3HT:$PC_{71}BM$ solutions. The large area of TEMT images for a,b) P3HT/$PC_{71}BM$, c,d) P3HT NWs/$PC_{71}BM$ **1**, and e,f) P3HT NWs/$PC_{71}BM$ **2** blend films; (a,c,e) before and (b,d,f) after light irradiation for 24 hr.

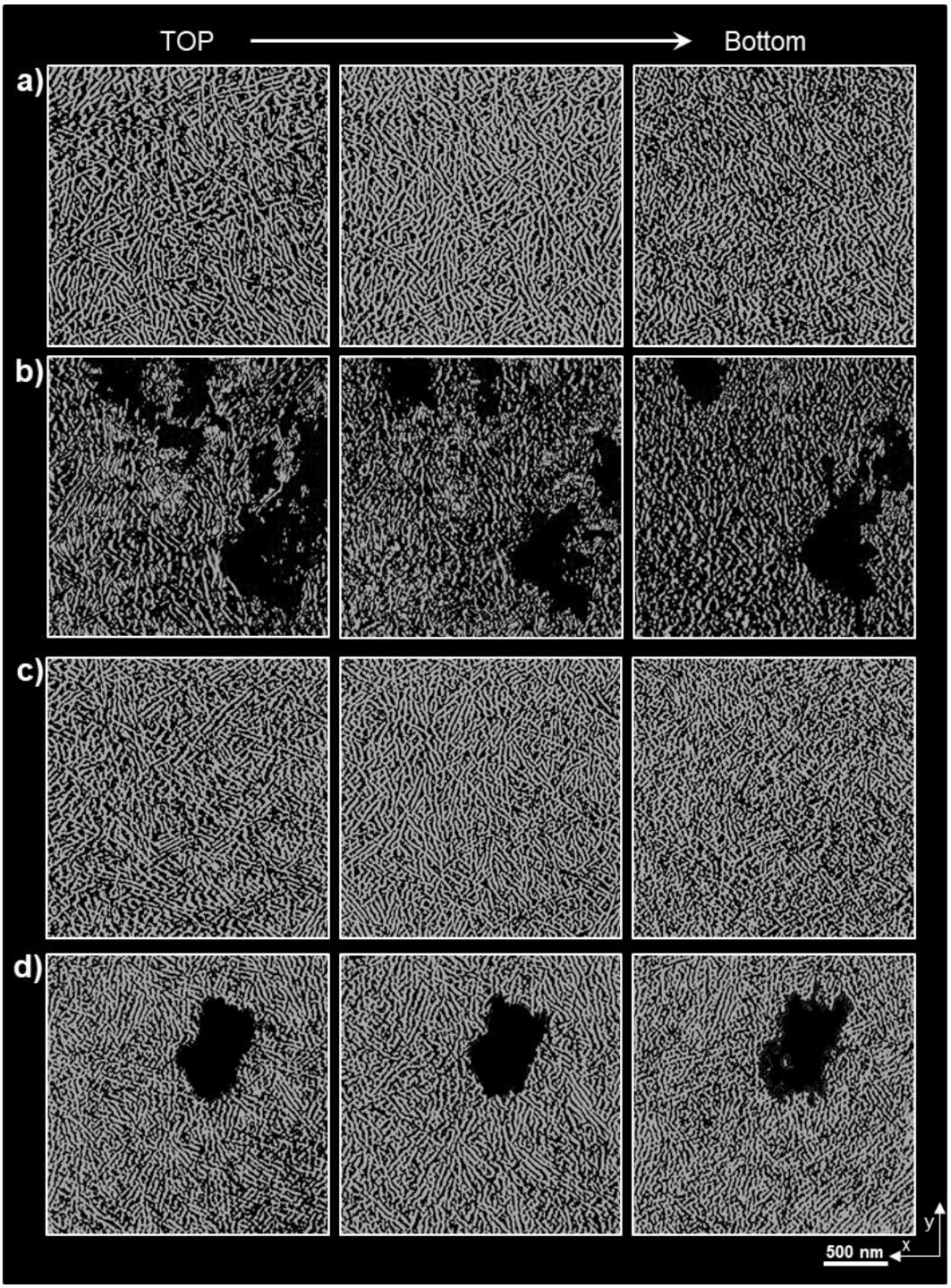

Fig. S7 The xy-slices from top to bottom extracted from 3D construction (as shown in Fig. S6) of both P3HT NWs/$PC_{71}BM$ a,b) **1** and c,d) **2** films: a,c) before and b,d) after light irradiation for 24 hr. The P3HT- and $PC_{71}BM$-rich domains were represented in gray and black, respectively.

Table S4 Relative continuous polymer phase per unit area (%), which calculated from binarized images shown in Fig. S7.

Films \ Area (%)[a]	Top		Middle		Bottom	
	P3HT	$PC_{71}BM$	P3HT	$PC_{71}BM$	P3HT	$PC_{71}BM$
P3HT NWs/$PC_{71}BM$ **1**	52.11	47.89	56.77	43.23	54.36	45.64
P3HT NWs/$PC_{71}BM$ **1** (after light irradiation)	30.60	69.40	35.35	64.65	34.91	65.09
P3HT NWs/$PC_{71}BM$ **2**	53.18	46.82	56.56	43.44	53.84	46.16
P3HT NWs/$PC_{71}BM$ **2** (after light irradiation)	44.51	55.49	48.31	51.69	47.25	52.75

[a]Total area of a xy-slice is 4,687,225 nm^2

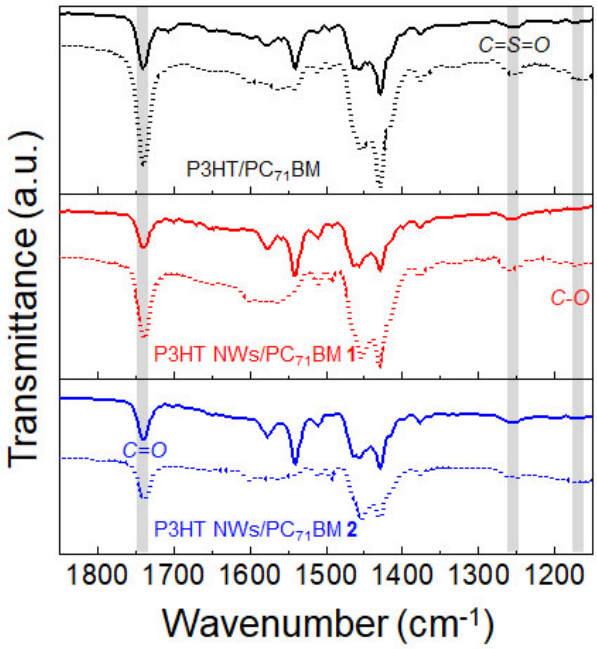

Fig. S8 FT-IR spectra of conventional P3HT/$PC_{71}BM$ film and NWs-based P3HT NWs/$PC_{71}BM$ films before (solid line) and after (dot line) exposure to light for 24 hr.

Tables S5-8 Summary of the volume fraction and composition of each phase in the examined samples.

Table S5 Calculated P3HT and $PC_{71}BM$ domains in P3HT NWs/$PC_{71}BM$ thin film **1** before light irradiation (from subtomogram of Fig. 3a).

Number of sub-tomogram	Volume fraction of P3HT (%)	Volume fraction of $PC_{71}BM$ (%)	Total volume (nm^3)	Volume of P3HT (nm^3)	Volume of $PC_{71}BM$ (nm^3)
1	50.19	49.81	2,019,888	1,013,772	1,006,116
2	54.36	45.64	2,019,888	1,098,086	921,802
3	53.33	46.67	2,019,888	1,077,251	942,637
4	51.99	48.01	2,019,888	1,050,182	969,706
5	55.40	44.60	2,019,888	1,119,054	900,834
6	52.21	47.79	2,019,888	1,054,664	965,224
7	55.71	44.29	2,019,888	1,125,332	894,556
8	53.57	46.43	2,019,888	1,081,955	937,933
9	48.65	51.35	2,019,888	982,619	1,037,269
10	50.02	49.98	2,019,888	1,010,265	1,009,623
11	47.59	52.41	2,019,888	961,188	1,058,700
12	51.25	48.75	2,019,888	1,035,156	984,732
13	53.58	46.42	2,019,888	1,082,286	937,602
14	53.42	46.58	2,019,888	1,079,061	940,828
15	54.13	45.87	2,019,888	1,093,277	926,612
16	52.90	47.10	2,019,888	1,068,428	951,460
17	53.49	46.51	2,019,888	1,080,339	939,549
18	52.41	47.59	2,019,888	1,058,674	961,214
19	55.79	44.21	2,019,888	1,126,797	893,092
20	56.25	43.75	2,019,888	1,136,155	883,733

Table S6 Calculated P3HT and $PC_{71}BM$ domains in P3HT NWs/$PC_{71}BM$ thin film **1** after light irradiation (from subtomogram of Fig. 3b).

Number of sub-tomogram	Volume fraction of P3HT (%)	Volume fraction of $PC_{71}BM$ (%)	Total volume (nm^3)	Volume of P3HT (nm^3)	Volume of $PC_{71}BM$ (nm^3)
1	33.39	66.61	2,019,888	674,406	1,345,482
2	32.54	67.46	2,019,888	657,320	1,362,568
3	35.28	64.72	2,019,888	712,701	1,307,187
4	34.53	65.47	2,019,888	697,459	1,322,429
5	32.64	67.36	2,019,888	659,296	1,360,593
6	33.95	66.05	2,019,888	685,700	1,334,189
7	27.56	72.44	2,019,888	556,586	1,463,302
8	39.60	60.40	2,019,888	799,791	1,220,097
9	34.42	65.58	2,019,888	695,239	1,324,649
10	36.64	63.36	2,019,888	740,016	1,279,872
11	34.00	66.00	2,019,888	686,853	1,333,035
12	34.15	65.85	2,019,888	689,818	1,330,070
13	32.58	67.42	2,019,888	658,162	1,361,726
14	34.39	65.61	2,019,888	694,553	1,325,336
15	31.58	68.42	2,019,888	637,966	1,381,923
16	32.55	67.45	2,019,888	657,445	1,362,443
17	33.15	66.85	2,019,888	669,688	1,350,200
18	33.49	66.51	2,019,888	676,368	1,343,521
19	38.95	61.05	2,019,888	786,781	1,233,107
20	37.54	62.46	2,019,888	758,290	1,261,598

Table S7 Calculated P3HT and $PC_{71}BM$ domains in P3HT NWs/$PC_{71}BM$ thin film **2** before light irradiation (from subtomogram of Fig. 3c).

Number of sub-tomogram	Volume fraction of P3HT (%)	Volume fraction of $PC_{71}BM$ (%)	Total volume (nm^3)	Volume of P3HT (nm^3)	Volume of $PC_{71}BM$ (nm^3)
1	50.93	49.07	2,019,888	1,028,638	991,250
2	50.42	49.58	2,019,888	1,018,498	1,001,390
3	50.69	49.31	2,019,888	1,023,889	995,999
4	51.85	48.15	2,019,888	1,047,298	972,590
5	50.60	49.40	2,019,888	1,022,092	997,797
6	49.79	50.21	2,019,888	1,005,694	1,014,194
7	52.97	47.03	2,019,888	1,069,929	949,960
8	52.72	47.28	2,019,888	1,064,796	955,092
9	53.81	46.19	2,019,888	1,086,859	933,029
10	54.53	45.47	2,019,888	1,101,429	918,459
11	51.80	48.20	2,019,888	1,046,211	973,677
12	48.58	51.42	2,019,888	981,163	1,038,726
13	51.54	48.46	2,019,888	1,041,099	978,789
14	49.01	50.99	2,019,888	990,012	1,029,876
15	51.90	48.10	2,019,888	1,048,318	971,570
16	51.88	48.12	2,019,888	1,047,847	972,041
17	48.54	51.46	2,019,888	980,478	1,039,410
18	52.54	47.46	2,019,888	1,061,274	958,615
19	53.81	46.19	2,019,888	1,086,859	933,029
20	55.51	44.49	2,019,888	1,121,297	898,592

Table S8 Calculated P3HT and $PC_{71}BM$ domains in P3HT NWs/$PC_{71}BM$ thin film **2** after light irradiation (from subtomogram of Fig. 3d).

Number of sub-tomogram	Volume fraction of P3HT (%)	Volume fraction of $PC_{71}BM$ (%)	Total volume (nm^3)	Volume of P3HT (nm^3)	Volume of $PC_{71}BM$ (nm^3)
1	40.02	59.98	2,019,888	808,289	1,211,600
2	42.82	57.18	2,019,888	864,823	1,155,065
3	46.54	53.46	2,019,888	940,084	1,079,804
4	48.22	51.78	2,019,888	973,921	1,045,967
5	46.22	53.78	2,019,888	933,673	1,086,215
6	44.21	55.79	2,019,888	892,958	1,126,930
7	51.74	48.26	2,019,888	1,045,056	974,832
8	50.86	49.14	2,019,888	1,027,240	992,648
9	48.54	51.46	2,019,888	980,379	1,039,509
10	43.77	56.23	2,019,888	884,150	1,135,739
11	41.17	58.83	2,019,888	831,497	1,188,391
12	42.18	57.82	2,019,888	851,959	1,167,930
13	43.55	56.45	2,019,888	879,568	1,140,320
14	47.65	52.35	2,019,888	962,505	1,057,383
15	48.52	51.48	2,019,888	980,139	1,039,750
16	47.62	52.38	2,019,888	961,919	1,057,969
17	43.76	56.24	2,019,888	883,875	1,136,013
18	49.01	50.99	2,019,888	989,994	1,029,895
19	48.56	51.44	2,019,888	980,904	1,038,984
20	48.99	51.01	2,019,888	989,467	1,030,422

Table S9 Summary of calculated P3HT and $PC_{71}BM$ domains in P3HT NWs/$PC_{71}BM$ **1** and **2** thin films before and after light irradiation (averaged over 20 subtomogram of Table S5-8).

Films	Volume fraction of P3HT (%)	Volume fraction of $PC_{71}BM$ (%)	Total volume (nm^3)	Volume of P3HT (nm^3)	Volume of $PC_{71}BM$ (nm^3)
P3HT NWs/$PC_{71}BM$ **1**	52.8	47.2	2,019,888	1,066,727	953,161
P3HT NWs/$PC_{71}BM$ **1** (after light irradiation)	34.1	65.9	2,019,888	689,722	1,330,166
P3HT NWs/$PC_{71}BM$ **2**	51.7	48.3	2,019,888	1,043,684	976,204
P3HT NWs/$PC_{71}BM$ **2** (after light irradiation)	46.2	53.8	2,019,888	933,120	1,086,768

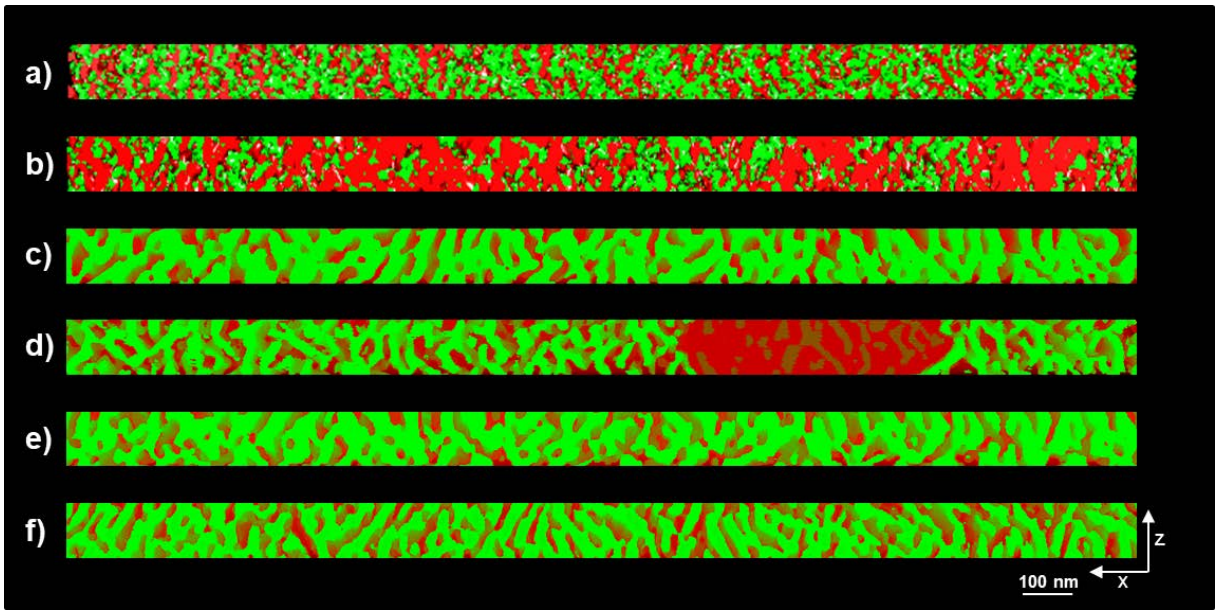

Fig. S9 Binarized xz-slice images extracted from 3D tomographic volume: of a,b**)** P3HT/$PC_{71}BM$ blend film and NWs-based films of c,d) P3HT NWs/$PC_{71}BM$ **1**, e,f) P3HT NWs/$PC_{71}BM$ **2**: a,c,e) before, and b,d,f) after light irradiation.

Table S10 Calculated P3HT and $PC_{71}BM$ domains from Fig. S9.

Films	P3HT (nm^2)	$PC_{71}BM$ (nm^2)	Total area (nm^2)
P3HT NWs/$PC_{71}BM$ **1**	144,570	91,270	235,840
P3HT NWs/$PC_{71}BM$ **1** (after light irradiation)	105,609	130,231	235,840
P3HT NWs/$PC_{71}BM$ **2**	137,589	98,251	235,840
P3HT NWs/$PC_{71}BM$ **2** (after light irradiation)	123,203	112,637	235,840

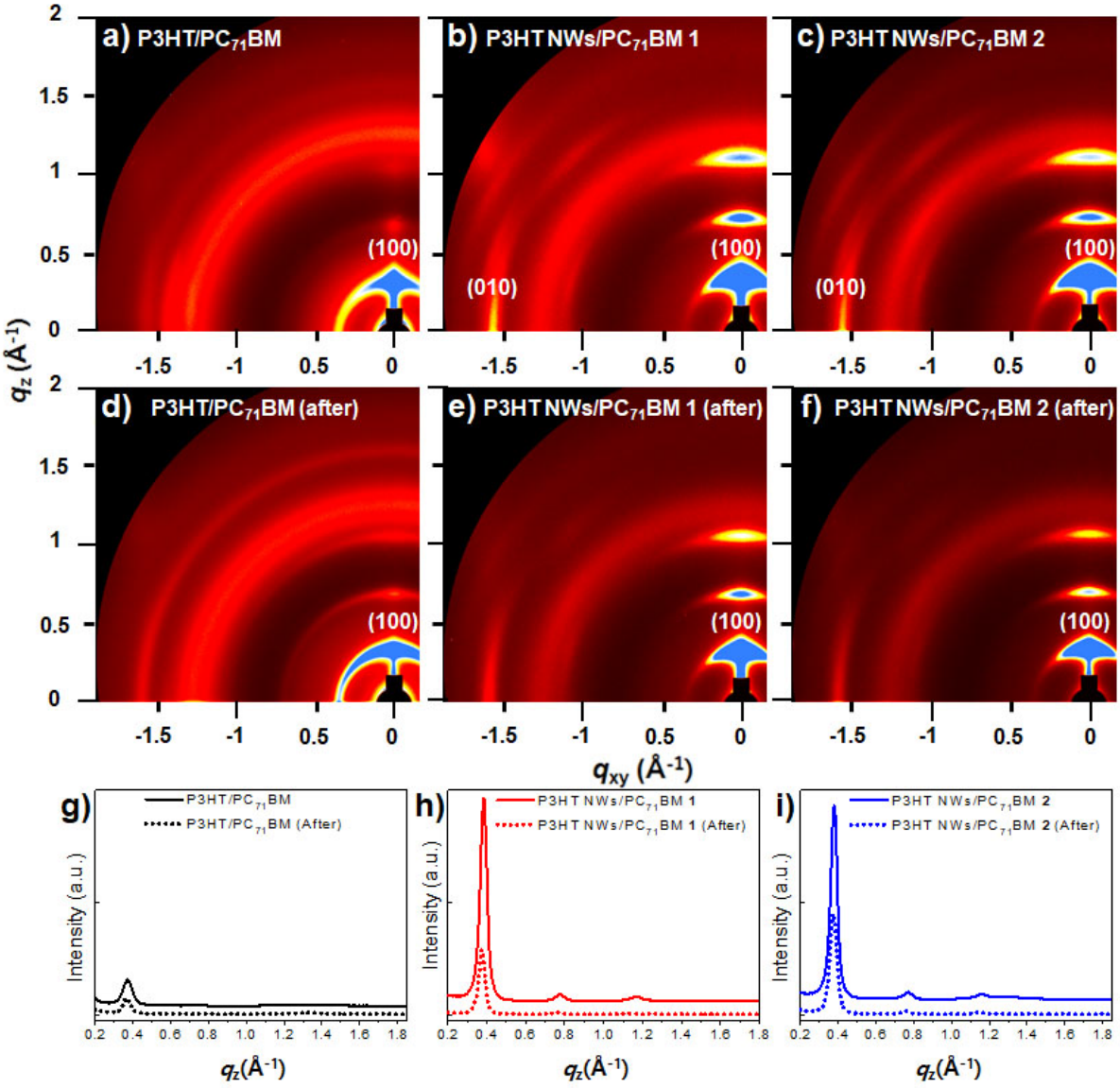

Fig. S10 GI-WAXS patterns of thin films as-cast from a,d) P3HT/$PC_{71}BM$, b,e) P3HT NWs/$PC_{71}BM$ **1**, and c,f) P3HT NWs/$PC_{71}BM$ **2** solutions; a-c) before and d-f) after light irradiation for 24 hr. g-i) Out-of-plane line cut (q_z) profiles from 2D GI-WAXS patterns of thin films as-cast from g) P3HT/$PC_{71}BM$, h) P3HT NWs/$PC_{71}BM$ **1**, and i) P3HT NWs/$PC_{71}BM$ **2** solutions before and after light irradiation for 24 hr.

Table S11 The *d*-spacing and relative crystallinity obtained from out-of-plane and in-plane GI-WAXS profiles of thin films as-cast from solutions.

Films	Out-of-Plane *d*-spacing (Å)	In-Plane *d*-spacing (Å)	Rel. Crystallinity
P3HT/$PC_{71}BM$	16.94	3.85	2.11
P3HT/$PC_{71}BM$ (after light irradiation)	17.15	3.80	1
P3HT NWs/$PC_{71}BM$ **1**	16.36	3.84	14.05
P3HT NWs/$PC_{71}BM$ **1** (after light irradiation)	16.94	3.77	6.61
P3HT NWs/$PC_{71}BM$ **2**	16.44	3.85	11.07
P3HT NWs/$PC_{71}BM$ **2** (after light irradiation)	16.96	3.79	8.08

Table S12 Photovoltaic parameters[a] of P3HT:$PC_{71}BM$ active layer films as a function of photo-aging time under 100 mW/cm^2 AM 1.5 G from a xenon arc lamp.

Films	Light irradiation time (hours)	V_{OC} (V)	J_{SC} (mA/cm^2)	*FF* (%)	PCE (%)
P3HT/$PC_{71}BM$	0	0.58	8.77	63	3.20
	1	0.57	8.69	64	3.15
	3	0.57	8.53	63	2.99
	5	0.56	8.12	61	2.78
	7	0.56	7.95	60	2.69
	10	0.56	7.80	57	2.50
	20	0.55	6.91	59	2.23
	40	0.54	6.41	56	1.93
P3HT NWs/$PC_{71}BM$ **1**	0	0.57	9.84	66	3.69
	1	0.57	9.63	67	3.67
	3	0.56	9.43	66	3.49
	5	0.56	9.27	66	3.45
	7	0.57	9.09	67	3.46
	10	0.56	8.73	66	3.26
	20	0.57	8.57	66	3.20
	40	0.56	8.49	63	2.95
P3HT NWs/$PC_{71}BM$ **2**	0	0.57	9.47	65	3.51
	1	0.57	9.34	65	3.49
	3	0.57	8.90	65	3.30
	5	0.57	8.72	65	3.25
	7	0.57	8.83	64	3.21
	10	0.57	8.62	65	3.21
	20	0.56	8.22	65	3.05
	40	0.56	7.84	63	2.76

[a]Inverted device architecture is ITO/ZnO NPs/PEIE/active layer (d = ~100nm)/MoO_3/Ag was used.

Video S1-S3

Video S1 A video of reconstructed 3D volume showing a comparison of the morphology changes of P3HT NWs/$PC_{71}BM$ **1** and **2** thin films by light irradiation.

Video S2 A video of reconstructed 3D volume of a P3HT NWs/$PC_{71}BM$ **1** thin film showing the morphological change by light irradiation.

Video S3 A video of reconstructed 3D volume of a P3HT NWs/$PC_{71}BM$ **2** thin film showing the morphological change by light irradiation.

4. References for Supporting Information

S1. C. Scharsich, R. H. Lohwasser, M. Sommer, U. Asawapirom, U. Scherf, M. Thelakkat, D. Neher, A. Köhler, *J. Polym. Sci., Part B: Polym. Phys.,* 2012, **50**, 442.

S2. G. Nagarjuna, M. Baghgar, J. A. Labastide, D. D. Algaier, M. D. Barnes, D. Venkataraman, *ACS Nano,* 2012, **6**, 10750.

S3. J. Clark, J.-F. Chang, F. C. Spano, R. H. Friend, C. Silva, *Appl. Phys. Lett.,* 2009, **94**, 163306.

S4. B. J. Tremolet de Villers, K. A. O'Hara, D. P. Ostrowski, P. H. Biddle, S. E. Shaheen, M. L. Chabinyc, D. C. Olson, N. Kopidakis, *Chem. Mater.,* 2016, **28**, 876.

S5. C. R. Singh, G. Gupta, R. Lohwasser, S. Engmann, J. Balko, M. Thelakkat, T. Thurn-Albrecht, H. Hoppe, *J. Polym. Sci., Part B: Polym. Phys.*, 2013, **51**, 943.

S6. X. Shen, V. V. Duzhko, T. P. Russell, *Adv. Energy Mater.,* 2013, **3**, 263.

S7. K. J. Ihn, J. Moulton, P. Smith, *J. Polym. Sci., Part B: Polym. Phys.,* 1993, **31**, 735.

S8. F. C. Spano, *J. Chem. Phys.,* 2005, **122**, 23470.